

Conservative Scale Recomposition for Multiscale Denoising (The Devil is in the High Frequency Detail)*

Gabriele Facciolo[†], Nicola Pierazzo[†], and Jean-Michel Morel[†]

Abstract. In this paper we reconsider the class of patch based denoising algorithms and observe that they underperform at lower image frequencies. We solve this problem by operating them within a multiscale structure. Our main observation is that denoising algorithms cannot be trusted with the restoration of high frequency details in the image. Indeed, since denoising algorithms must impose their image prior, the fine details are either smoothed or sharpened in the result. In any case the high frequency properties of the images are altered. This realization has a profound implication on the multiscale approaches, which assume that coarse scale restorations are better denoised and hence are replaced in the finer resolutions. This leads to frequency cut-off artifacts as the coarse restorations are pasted at higher resolutions. We start by studying this phenomenon on a simple Discrete Cosine Transform (DCT) pyramid, for which the artifacts resulting from this process are evident. We propose a simple solution consisting of a “conservative recomposition” of the scales that only retains the lower frequencies of each scale, with the obvious exception of the scale at the highest resolution. This soft fusion eliminates the ringing artifacts and attenuates staircasing artifacts and low frequency bumps. An added benefit of the DCT pyramid is that it allows one to maintain the white noise at the lower resolutions, hence it can be combined with any denoising algorithm without adaptation. This soft fusion recipe can be generalized to any other pyramid structure. We apply it to a Laplacian pyramid as an example. Our proposal merges and operates any denoising algorithm into a multiscale method, with improvements both in visual quality and Peak Signal to Noise Ratio (PSNR), and with little additional complexity. The method is demonstrated on several classic or state-of-the-art denoising algorithms.

Key words. multiscale, image denoising

AMS subject classifications. 68Q25, 68R10, 68U05

DOI. 10.1137/17M1111826

1. Introduction. This paper addresses the issue of restoring low frequency detail in state-of-the-art denoising algorithms. We observed that these algorithms restrict their action to a limited neighborhood of each pixel. This implies that low frequency noise is not handled. As our technology is producing ever larger images, the low frequency noise becomes conspicuous in flat areas. Indeed, most recent image denoising algorithms are “patch based.” They typically process 8×8 patches and thereafter aggregate the results obtained on all patches containing

*Received by the editors January 17, 2017; accepted for publication (in revised form) July 12, 2017; published electronically September 26, 2017. This article is related to a companion publication [22]: N. Pierazzo, J.-M. Morel, and G. Facciolo, *Multi-scale DCT denoising*, IPOL Image Processing On Line, preprint, 2017.

<http://www.siam.org/journals/siims/10-3/M111182.html>

Funding: The work of the authors was partly founded by BPI France and Région Ile de France, in the framework of the FUI 18 Plein Phare project, the European Research Council (advanced grant Twelve Labours 246961), the Office of Naval Research (ONR grant N00014-14-1-0023), and ANR-DGA project ANR-12-ASTR-0035.

[†]CMLA, ENS Paris Saclay, Cachan, 94230, France (gfaciol@gmail.com, nicolapierazzo@gmail.com, moreljeanmichel@gmail.com).

each given pixel. This technique does not naturally include a multiscale image representation.

Restoring a universal multiscale principle applicable to all image denoising algorithms has already been explored in [2, 8]. Even though the results of these papers are only partially satisfying (as we shall see), their approach is simple and promising. In the pyramid processing of [2] each level is denoised independently, similarly to what is proposed in the current paper. The difference is that at lower resolutions, the noise becomes correlated by the pyramid, thus potentially reducing the performance of standard algorithms. This method obtains PSNR gains for very high noise levels only. With the *conservative recomposition* introduced in this paper, we shall see that it is possible to obtain gains at all noise levels (section 2).

Another multiscale model was proposed in [27]. The difference with our work is that it does not use a classical denoising algorithm in the process and does not avoid artifacts in the reconstruction. The most recent work proposing a multiscale version of a state-of-the-art restoration algorithm is probably [21], which proposes a two-scale extension of EPLL (Expected Patch Log Likelihood) [35] and demonstrates a moderate PSNR gain. EPLL is an “external denoising” method based on a Gaussian mixture prior learned from a large patch database. Its variational formulation permits a natural multiscale extension by using the same prior on the down-sampled image. This multiscale framework works, but is therefore limited to a particular algorithm and variational method. We shall compare the result of our nonspecific multiscale version of EPLL to the specific version in [21].

The multiscale representation is also intrinsically present in wavelet-based denoising algorithms [5, 9, 25, 19]. Wavelet thresholding is the pioneering multiscale image denoising method. Yet it has proved difficult to extend, and is currently surpassed by the more recent patch based methods. It nevertheless remains a source of inspiration, as recent methods have abandoned multiscale image representations. The wavelet methods all present annoying “ringing” or “butterfly” artifacts attributable to the transform coefficients thresholds causing Gibbs effects. A multiscale representation is also present in [30], where the K-Singular Value Decomposition (KSVD) algorithm is applied on a wavelet decomposition of the image. The improvement over a single scale KSVD is important, especially for high PSNR, but since the wavelet sub-bands are independently denoised, the authors need what they call a fusion strategy in order to reduce the artifacts. Another way to deal with these artifacts is to eliminate them after denoising. In [6] for example, the authors proposed to reduce ringing and butterfly effects in wavelet-based denoising by using a constrained total variation minimization.

Much effort has been devoted to the wavelet methods. They were the best performing methods in the beginning of the century and reached a high level of sophistication. The very complete endeavor made in the series of papers [28, 31, 29, 24, 26, 23, 12, 20, 10, 11] involves more and more complex multiscale wavelet denoising algorithms.

Their idea is to learn for each image a stochastic model for the noiseless “wavelet coefficient neighborhood” P for each wavelet sub-band and modality. The main underlying model for P is the Gaussian scale mixture (GSM), defined as $P = \sqrt{z}U$, where U is a zero-mean Gaussian random vector and z is an independent positive scalar random variable. The variable z represents the random “scale” of the wavelet coefficient. (Here the “scale” has to do with the variance of these coefficients, and not with a spatial scale.) In all the above mentioned papers, the wavelet coefficient neighborhood turns out to be a patch of an oriented channel of the image at a given scale, complemented with a coefficient of the channel at the same

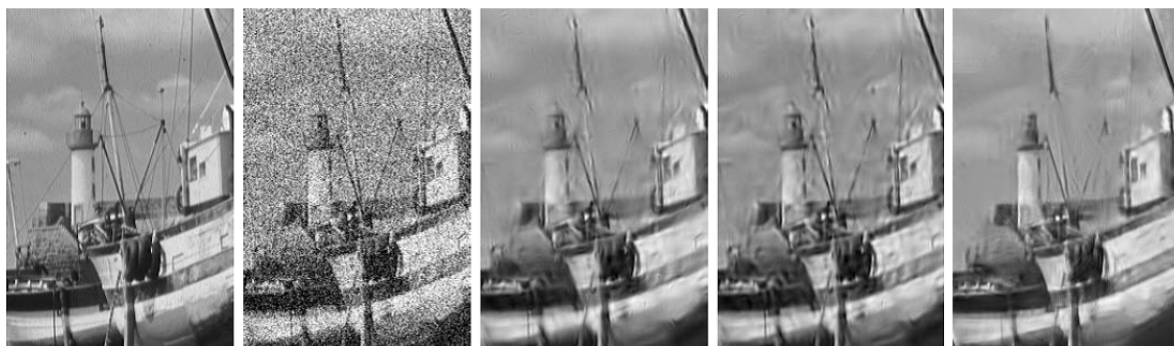


Figure 1. From left to right: original, noisy image ($\sigma = 50$); Gaussian scale mixture by Bayesian least squares [24] ($PSNR = 26.3$); fields of Gaussian scale mixtures [20], ($PSNR = 27.0$); and the proposed multiscale DCT pyramid applied to BM3D ($PSNR = 26.73$). In spite of their excellent PSNR performance, these methods suffer from severe ringing artifacts. Being inherently multiband, they cannot benefit from the conservative recomposition proposed here.

orientation and the next lower scale. To use the GSM model for wavelet patch denoising, the noisy input image is first decomposed into a wavelet pyramid, and each image of the pyramid is denoised by a Bayesian least square method. The resulting denoised image is obtained by the reconstruction algorithm from the wavelet coefficients. To avoid ringing artifacts in the reconstruction, a redundant version of the wavelet transform, the steerable pyramid, is used. More precisely, the image is decomposed in 18 pyramid subbands (4 orientations at each of 4 scales, plus high-pass and low-pass residuals). For each band (except the low-pass) the Bayesian denoising method is applied. Although the subbands are processed sequentially, they are not processed independently, since the conditioning neighborhoods include coefficients from coarser scales. The denoised image is computed by inverting the pyramid transform. The best efficiency seems to be reached with a 3×3 spatial block around each oriented wavelet coefficient, supplemented with one coefficient at the same location and at the next coarser scale with the same orientation [26]. Hence, the wavelet neighborhood size is 9 or 10.

In short, the most sophisticated wavelet methods, being fully multiscale, proceed by denoising sequentially (and causally) wavelet patches at each scale with the same process. A causal (from coarse to fine) interchannel correlation is involved, as the wavelet patches contain coefficients in the same orientation but at two different scales. The ultimate method of this class is proposed in the papers [10, 11], where neighborhoods of each subband are described as a finite mixture of GSMS. The mixing densities and covariance matrices associated with each of the GSM components from a single image have then to be learned and implicitly segment the image into regions of similar content.

The wavelet methods, being fully multiscale, proceed by denoising sequentially wavelet patches at each scale with the same process. A causal (from coarse to fine) interchannel correlation is involved as the wavelet patches contain coefficients in the same orientation but at two different scales. In spite of their excellent PSNR performance these methods suffer from severe ringing artifacts as illustrated in Figure 1. Being inherently multiband, these methods cannot benefit from the conservative recomposition proposed here.

Indeed, a main feature of the multiscale method introduced in [2] (and extended here) is

that it starts with *independent, redundant multiscale denoising*. The image itself is denoised (by a single scale denoising method, though). But all the down-sampled images are denoised by the same method as well. Thus, all lower levels of the pyramid are denoised more than once, which opens the way to a recombination of the various results, which are different. This is not applicable to the wavelet algorithms that we just considered. Indeed, they belong to the *causal* class: the denoised image at scale i is obtained by using the denoised image at the coarser scale $i + 1$. Thus, there is no redundancy in the denoising process. The same remark applies to the noise clinic [16], a multiscale blind patch based denoising algorithm which belongs to the causal class as defined above.

1.1. Our contribution. Our main observation is that denoising algorithms cannot be trusted with the restoration of high frequency details in the image. Indeed, since denoising algorithms must impose their image prior, the fine details are either smoothed or sharpened in the result. In any case the high frequency properties of the images are altered. This realization has a profound implication on the multiscale approaches which assume that coarse scale restorations are better denoised and hence are replaced in the finer resolutions. This leads to a sort of frequency cut-off artifact as the coarse restorations are pasted at higher resolutions. To address this issue we introduce a multiscale framework that can be applied to any existing single-scale denoising algorithm, consistently improving its results. The framework uses a simple DCT or Laplacian pyramid, and is not computationally demanding. We shall see that simply using a pyramid would lead to serious ringing artifacts. We solve this issue by introducing what we call a *conservative multiscale reconstruction*, which keeps the advantages of the pyramid while avoiding its problems.

Section 2 justifies and describes our proposed simple formalism for multiscale denoising with conservative recomposition. The application of this framework is first described on the DCT pyramid and then on the Laplacian pyramid. Section 3 examines how to apply this framework to several classic denoising algorithms. For each, the optimal parameters of the multiscale framework are first estimated. Section 4 is an extensive experimental evaluation. It computes the PSNR and Structural SIMilarity (SSIM) index gains obtained for each considered denoising method by the multiscale framework with the DCT and Laplacian pyramids. In both cases it evaluates the gain brought by the conservative recomposition. It also illustrates the visual quality gains of a multiscale method, which are in fact considerable and arguably better reflected by our SSIM measurements than by the steady but moderate PSNR gains.

This evaluation is performed on six classic denoising algorithms, starting with the very classic and elementary DCT denoising, for which the gain is considerable, continuing with a dictionary learning algorithm (KSVD), with an external denoising algorithm based on a Gaussian mixture prior (EPLL), with a pure patch based algorithm (Nonlocal Means) and ending with mixed strategies using patches and adaptive transform thresholding like BM3D and Nonlocal Bayes. In all, a significant PSNR gain is demonstrated.

This work was published jointly with the Image Processing On Line (IPOL) article [22], which thoroughly described the proposed method applied to the DCT denoising algorithm [34] and provides implementation details, source code, and an online demonstration.¹

¹See <http://www.ipol.im/pub/pre/201/>.

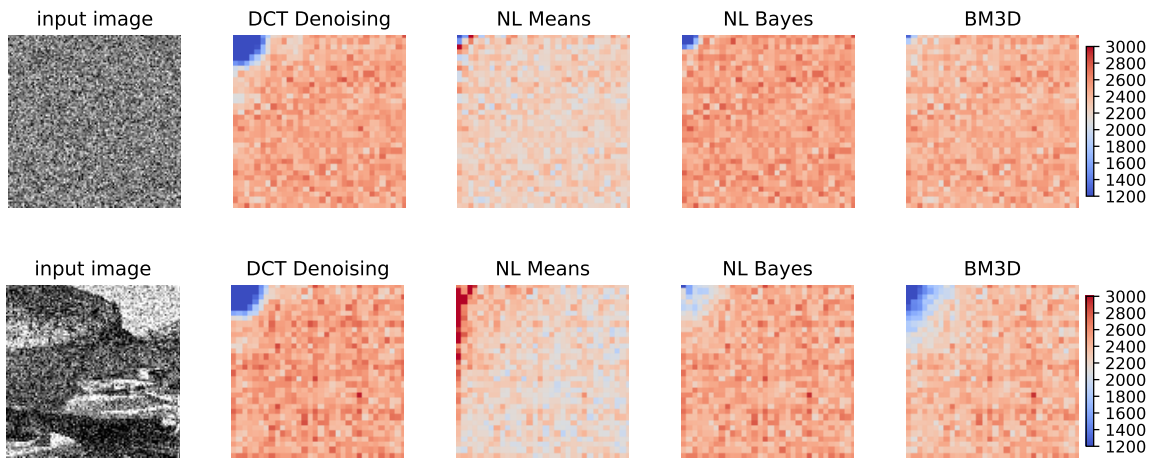


Figure 2. *DCT power spectrum of the extracted noise (noisy minus denoised) after denoising the image on the left (a pure white noise on the top and a real image on the bottom) with several algorithms. The perfect denoising algorithm would extract a pure white noise in both cases. The power spectra are binned for display and the noise standard deviation is $\sigma = 50$. Notice that the extracted noise tends to be uniform over the mid and high frequencies but has less power on the lower frequencies (upper-left corner of the power spectrum). This means that low frequency noise is less present in the residual. In the case of Nonlocal Means, the extracted noise contains more energy than expected in the low frequencies, meaning that some image structure has been removed by the denoising algorithm.*

2. A multiscale framework. We take the classic assumption [13] that the statistics of natural images are invariant to a change of scale. A possible justification for this is that scenes are equally likely to be viewed from different distances, and that the same objects in a given scene may also appear at any distance [18]. The scale invariance assumption is used for several multiscale algorithms, such as [25, 2]. In [36], natural images are modeled by a scale invariant dead leaves model.

Because of the limited size of patches and search windows, local and nonlocal denoising methods attack well high frequency noise, but underperform on low frequencies. This fact is easily checked by examining the power spectrum of the extracted noise after applying these methods. We call *extracted noise* the difference noisy image minus denoised result. Figure 2 shows the DCT power spectrum of the extracted noise of four popular denoising algorithms on an image composed only of white noise. A similar experiment on a natural image is also shown in Figure 2; in this case the residual not only contains the removed noise but also carries some image structure. As expected, the power of the extracted noise on the high frequencies is even, but drops on the low frequencies. This means that, to some extent, low frequency noise has not been seriously attacked by the denoising algorithm. Given a multiscale image representation, a straightforward way to improve the denoising performance on the low frequencies is to apply the denoising algorithm at each scale, and then to recompose the image, always preferring the low frequency coefficients estimated at lower resolutions. The image pyramid [3] for a noisy image x_1 can be generated by successively down-sampling it with

$$(1) \quad x_i = \text{REDUCE}(x_{i-1}),$$

where $\text{REDUCE}()$ denotes the combination of a low pass filter with down-sampling. Each noisy down-sampled image is then independently denoised using the very same denoising algorithm, yielding $y_i = \text{DENOISE}(x_i)$ at the i th level of the pyramid. The denoised pyramid is then recomposed starting from the low resolution images and substituting them into the higher resolution result ($i = n-2, \dots, 1$) as

$$(2) \quad z_i = \underbrace{y_i - \text{EXPAND}(\text{REDUCE}(y_i))}_{\text{high freq.}} + \underbrace{\text{EXPAND}(z_{i+1})}_{\text{low freq.}},$$

where $z_n = y_n$ and $\text{EXPAND}()$ denotes an up-sampling or interpolation operator. The final denoising result is given by z_1 . Let us observe that low resolution images are assumed to be perfect by this recombination; that is they are just pasted into the pyramid while the corresponding band of the high resolution image is removed.

The main problem with this recombination for denoising is that the low resolution denoised images might contain high frequency artifacts that will be up-sampled during the recombination. This leads to the apparition of Gibbs-like artifacts that are related to the construction of the pyramid itself.

We shall first observe and explain these artifacts on a simple DCT pyramid, for which the artifacts resulting from this process are evident. This will lead to proposing our solution, the *conservative recombination* as a “soft fusion” of the scales that only retains the lower frequencies of each scale, with the obvious exception of the scale at the highest resolution. An added benefit of the DCT pyramid is that it allows one to maintain the white noise at the lower resolutions, which, hence, can be combined with any denoising algorithm without adaptation. Then the concept of *conservative recombination* will be generalized to any multiscale scheme, and concretely to the Laplacian multiscale scheme proposed in [2].

2.1. The DCT pyramid. The Discrete Cosine Transform, or DCT, given in (3) is a real separable orthogonal transform. For two-dimensional (2-D) signals, the DCT can be computed by applying (3) to the rows and the columns. Its inverse is the IDCT (4),

$$(3) \quad Y_k = \frac{1}{N} \sum_{j=0}^{N-1} X_j \cos \left[\pi \left(j + \frac{1}{2} \right) \frac{k}{N} \right],$$

$$(4) \quad X_k = Y_0 + 2 \sum_{j=1}^{N-1} Y_j \cos \left[\pi \left(k + \frac{1}{2} \right) \frac{j}{N} \right].$$

The DCT is classically preferable to the DFT because it avoids ringing effects at the image boundaries.

The DCT transform can be used to form a multiscale representation of an image. The down-sampling of the image is simply done by extracting the low frequencies from the DCT transform of the image, and then computing the IDCT on just those frequencies. Conversely, up-sampling is done by zero padding, so the recombination equation (2) reduces to replacing the low frequencies of an image with those coming from a coarser scale. In a dyadic pyramid each layer of the pyramid has half the width and half the length of the previous one. Using

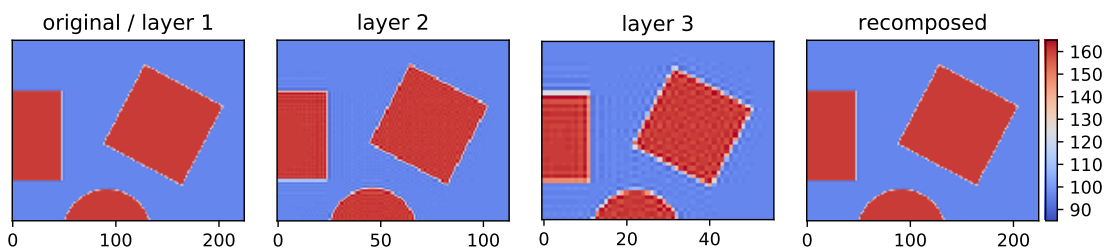


Figure 3. Illustration of the ringing artifacts in the coarser levels of the DCT pyramid using a synthetic image. Since keeping all the coefficients in the low frequency of the DCT is comparable to a convolution with a sinc function, the ripples are visible in the coarser resolutions (layers 2 and 3). The layers are resized and the contrast stretched for easier visualization.

(3) and (4) for this procedure keeps the values of the image on the same range. On the other hand, the standard deviation of the noise gets halved at each successive scale.

This representation has the advantage that since an additive white Gaussian noise remains so under the DCT transform, the model of the noise remains the same in every layer of the pyramid. Thus, no particular adaptation of the initial single scale denoising algorithm is needed to denoise the coarse (low resolution) layers. This is an important property, since it allows a straightforward extension of any denoising algorithm. Recomposing the pyramid is trivial, since it can be reduced to substituting the low frequencies of a layer with the frequencies of the coarser layer.

The drawback of this model is that since each layer is essentially the result of the convolution of the previous (high resolution) one with a sinc-like function, ringing artifacts due to the Gibbs effect unavoidably appear in the coarser layers. Figure 3 illustrates these artifacts on the first three levels of a DCT pyramid of a synthetic image. These artifacts are a necessary part of the pyramid representation. Once recomposed with (2) they cancel-out. The problem with denoising is that the Gibbs artifacts are also present in the pyramid of a noisy image. Since they generally have a low local amplitude compared to the noise, the denoising algorithm generally removes them, as illustrated in Figure 4.

2.2. A conservative pyramid recomposition. We have seen that ringing artifacts appear in the pyramid, but also that they disappear by cancellation during recomposition. Indeed, Gibbs effects in the DCT Pyramid are compensated by the complementary oscillations resulting from the high passed images (as shown in Figure 3). Our problem is that the high frequency oscillations of the low-resolution images are likely to be damaged or even removed by the denoising method. Then in a naive recomposition the oscillations resulting from the high-pass will no longer be compensated and the Gibbs effect appears, as seen in the second row of Figure 4.

To solve this issue, we found an easy and arguably new solution. We observe that the original single scale algorithm is applied to the whole image, and therefore to all frequencies. But it is also applied to the down-sampled images. Thus we have two different denoised estimates for the image low frequencies. Hence, the damages done by the denoising on the (needed!) Gibbs effects can be avoided by discarding the higher frequencies of the denoised down-sampled

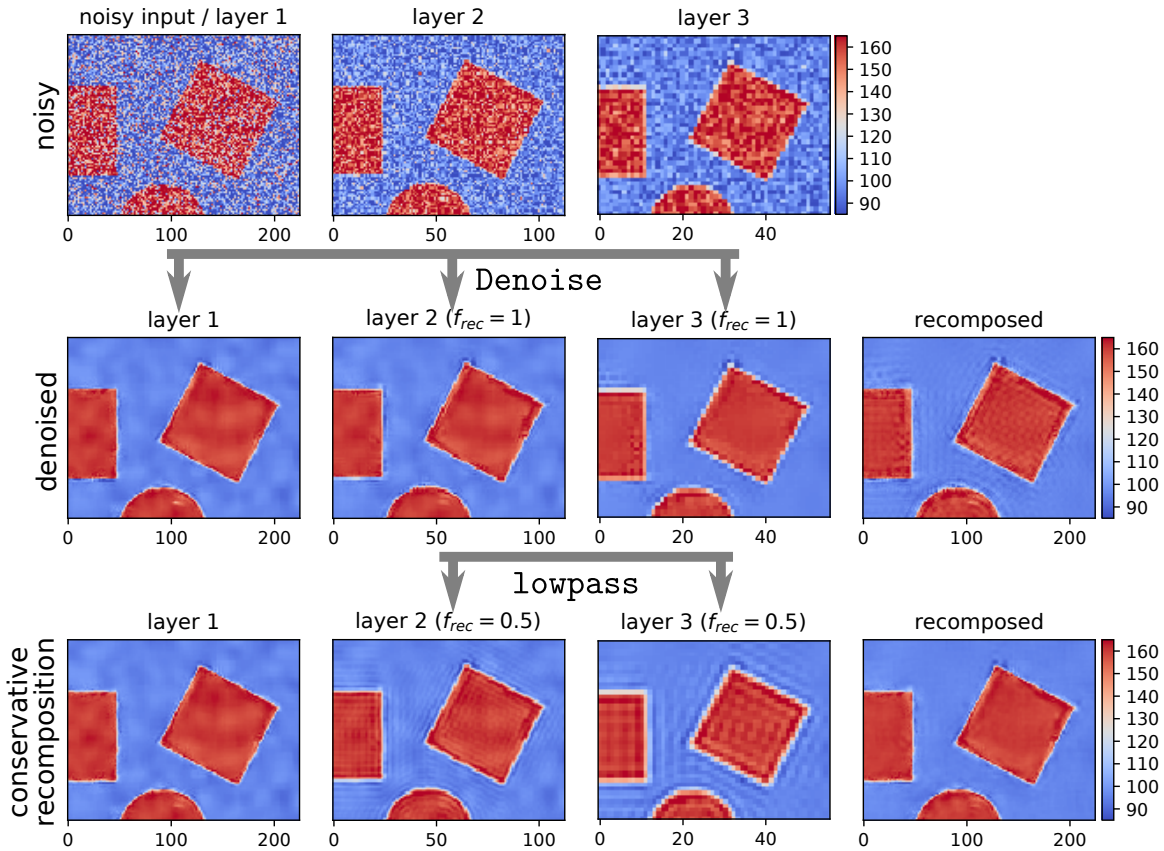


Figure 4. *DCT pyramid of a noisy image ($\sigma = 30$); layers 1 and 2 are down-scaled by DCT. The noiseless image is shown in Figure 3. The second row shows the denoising results of the single-scale Nonlocal (NL)-Bayes applied to each one of the layers. Note that in the denoised images most of the ringing visible in Figure 3 is not present. This spells doom for the recomposed pyramid as the ringing resulting from high-pass filtering is no longer compensated, as seen in the recomposition column. The third row illustrates how conservative recombination works. Applying a low pass filter to layers 1 and 2 of the denoised image restores the ringing in the coarse layers. Hence, the conservative recombination (depicted in Figure 5) discards the high frequencies of the coarse layers so that the result has fewer artifacts.*

image, to replace them by the corresponding medium frequencies of the denoised higher resolution layer (as shown in the last row of Figure 4). This conservative pyramid recomposition can be expressed more formally by introducing a low-pass filtering of the low resolution image $\text{LOWPASS}(z_i, f_{\text{rec}})$ in (2), resulting in

$$(5) \quad z_i = y_i - \text{EXPAND}(\text{LOWPASS}(\text{REDUCE}(y_i), f_{\text{rec}})) + \text{EXPAND}(\text{LOWPASS}(z_{i+1}, f_{\text{rec}})),$$

where $f_{\text{rec}} \in [0, 1]$ controls the fraction of low frequencies being preserved in the recomposition.

In short, we keep only the *lower frequencies* of the coarser layers (except of course for the highest resolution), as detailed in section 2.3. The width of the overlap frequency band, where the high resolution layer is preferred, will be specific for each single-scale denoising algorithm. As we will see in section 2.4, this strategy is not specific to the DCT pyramid and can be extended to any other pyramid structure.

Algorithm 1 Pseudocode for the multiscale framework.

```

1: function MULTISCALE( input,  $\sigma_{noise}$ ,  $n_{scales}$ ,  $f_{rec}$ ,  $s$  )
   Input: input noisy image
   Input:  $\sigma_{noise}$  noise standard deviation
   Input:  $n_{scales}$  number of scales
   Input:  $f_{rec}$  recombination factor of the DCT Pyramid ( $\gamma$  for Laplacian Pyramid)
   Input:  $s$  current scale in the recursion (default 1, for the outer call)
   Output: denoised image
2:    $y \leftarrow \text{DENOISE}( \text{input}, \sigma_{noise}/2^{s-1} )$                                  $\triangleright$  Call the denoising algorithm
3:   if  $s = n_{scales}$  then                                          $\triangleright$  The current scale is the last one
4:     return y
5:    $z \leftarrow \text{MULTISCALE}( \text{REDUCE}( \text{input}), \sigma_{noise}/2^s, n_{scales}, f_{rec}, s+1 )$      $\triangleright$  Recursion
6:    $H \leftarrow y - \text{EXPAND}( \text{LOWPASS}( \text{REDUCE}(y), f_{rec} ) )$ 
7:    $L \leftarrow \text{EXPAND}( \text{LOWPASS}(z, f_{rec}) )$ 
8:   return  $H + L$ 

```

2.3. Conservative recombination for the DCT pyramid. A recursive pseudocode for our proposed multiscale framework is shown in Algorithm 1, and a scheme showing the procedure for the DCT pyramid on a sample image is shown in Figure 5. In Algorithm 1, the level 1 corresponds to the input image itself, and every other level is half the size of the previous one. The call $\text{MULTISCALE}(\text{input}, \sigma_{noise}, n_{scales}, f_{rec}, 1)$ performs the whole denoising process on the *input* image. Here, $\text{DENOISE}(image, \sigma)$ is the denoising algorithm that is being immersed in the multiscale framework. The function $\text{LOWPASS}(x, f_{rec})$ just sets to zero the $1 - f_{rec}$ highest frequencies of the DCT representation of *x* and returns the resulting image. So the low frequency coefficients of *input* get replaced at each scale by those from the coarser scale *z* in a ratio proportional to f_{rec} .

Since each layer of the pyramid contains a quarter of the pixels of the previous one, by assuming a linear time-complexity for the denoising algorithm with respect to the image's size, the additional complexity to denoise the whole pyramid is less than one-third of the single-scale denoising complexity. The factor $4/3$ comes as an approximation of the full pyramid, being the limit of the infinite sum of 4^{-k} . We observed in our experiments that the pyramid overhead is mainly due to the DCT transform, which is nevertheless fast to compute [33].

2.4. Conservative recombination for the Laplacian pyramid. We now show that the very same process that we have just developed for the DCT pyramid adapts to any other pyramid. The authors of [2] proposed a denoising meta-procedure that operates on a Laplacian pyramid. They apply any existing denoising algorithm at different scales of the pyramid and recombine the resulting images into a single denoised image following (2). For resizing the images ($\text{REDUCE}()$ and $\text{EXPAND}()$) they used a windowed sinc kernel (Lanczos-3), which is almost diagonal in the frequency domain. They mention that the choice of the interpolation kernel is not critical for the final result. A potential drawback of a multiscale procedure based on Gaussian down-sampling is that the whiteness property of the noise may not be preserved by the down-sampling operations.

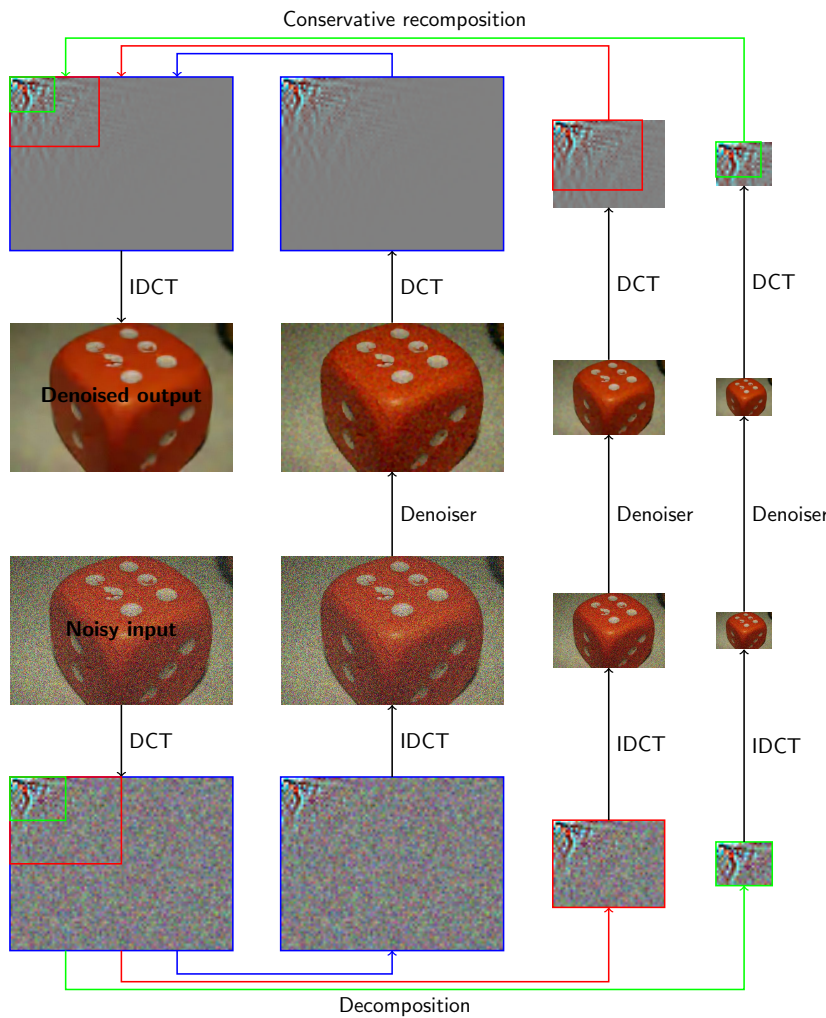


Figure 5. Scheme of our multiscale framework with conservative recomposition, shown with three levels. Notice that not all the frequencies of the upper layers are used for the recomposition. This is done in order to avoid ringing artifacts. The single denoising steps can be performed by any existing denoising algorithm (in this illustration, DCT Denoising [34]).

The authors of [2] studied the improvement obtained by their multiscale meta-procedure for increasingly higher noise levels (up to $\sigma = 200$ for grayscale images). They observed that at very high noise levels this improvement stagnated. This is because at very high noise levels, the single-scale denoising algorithms become ineffective and start “polluting” the output. Their proposed solution consists of removing these “uncertain” high frequency contributions by thresholding them. The reconstruction formula with thresholding then becomes

$$(6) \quad z_i = \mathcal{T}(y_i - \text{EXPAND}(\text{REDUCE}(y_i)), \lambda) + \text{EXPAND}(y_{+1}),$$

where $\mathcal{T}(y_i - \text{EXPAND}(\text{REDUCE}(y_i)), \lambda)$ is the hard-thresholding operator, with threshold λ applied to the high frequency component of the result. In practice, the threshold is tuned for

each algorithm to kick-in at very high noise levels, effectively dropping the contribution of the finer scales, leaving as the result the up-sampled version of an image denoised at a lower scale. This indeed yields an improvement of the result, but is a sort of Pyrrhic victory, being only due to the zoom out and therefore to a straight loss of resolution. Here, we shall therefore not be considering the threshold operation.

Bringing conservative recombination to the Laplacian pyramid meta-procedure. Our main observation here follows. The multiscale method [2] is based on a pyramidal scheme that is structurally similar to the DCT pyramid proposed in the current paper. Thus, it is straightforward to incorporate our conservative recombination into it. Note that the equivalent of the DCT ringing artifacts for the Lanczos-3 interpolation are more localized perhaps, but still present. The down-sampling operation can introduce aliases or oversmooth the result. But in any case these artifacts are subtle, and a denoising algorithm will likely alter or remove them, thus altering the coherence of the pyramid in a similar manner than with the DCT ringing artifacts.

We observe that the conservative recombination amounts to low-passing the lower resolution levels of the denoised pyramid to restore the coherence across the pyramid. Here, by involving a Gaussian kernel g_γ as our low-pass filter we can define the conservative recombination for the Laplacian pyramid by

$$(7) \quad z_i = y_i - \text{EXPAND}(g_\gamma * \text{REDUCE}(y_i)) + \text{EXPAND}(g_\gamma * y_{+1}),$$

where the spread γ is the analogue of f_{rec} in Algorithm 1. The experiments in section 4 illustrate the improvement resulting from applying this conservative recombination with kernel g_γ to the framework of [2]. We will also discuss the optimal choice for γ in this conservative recombination.

3. Application to multiscale versions of classic algorithms. We applied the proposed multiscale framework to six classic denoising algorithms using the DCT or the Laplacian pyramids. The only parameters of the framework are the number of scales and the recombination factor (either f_{rec} , or g_γ). For each algorithm, we evaluated the effect of the parameters of the framework for a choice of realistic noise levels, using the set of training images shown in Figure 6. The internal parameters of the single-scale algorithms were not modified. The best parameters for each algorithm and noise level (shown in Figure 7 for the DCT pyramid and in Figure 8 for the Laplacian pyramid) were then selected as those leading to the highest average PSNR gains. Similar conclusions were obtained with the SSIM [32] index (not shown).

Note that in Figure 7 the recombination factor is inactive on the right-most columns of the plots ($f_{rec} = 1.0$). In contrast, the recombination factor is inactive in Figure 8 with $g_\gamma = 0.0$. Thus the leftmost column of the plots coincides with the choice used in [2].

Nonlocal means. The paper [1] includes one of the first methods that exploited the patch selfsimilarities in the images. Notice that different levels of noise call for different parameters (notably for $\sigma = 10$). This was to be expected, as the denoising algorithm's internal parameters depend on the noise level.

K-SVD denoising. The papers [7, 17] contain an effective method that uses sparse representations of the image patches in terms of a learned dictionary.

DCT denoising. The paper [34] consists of a threshold of a patchwise DCT of the image

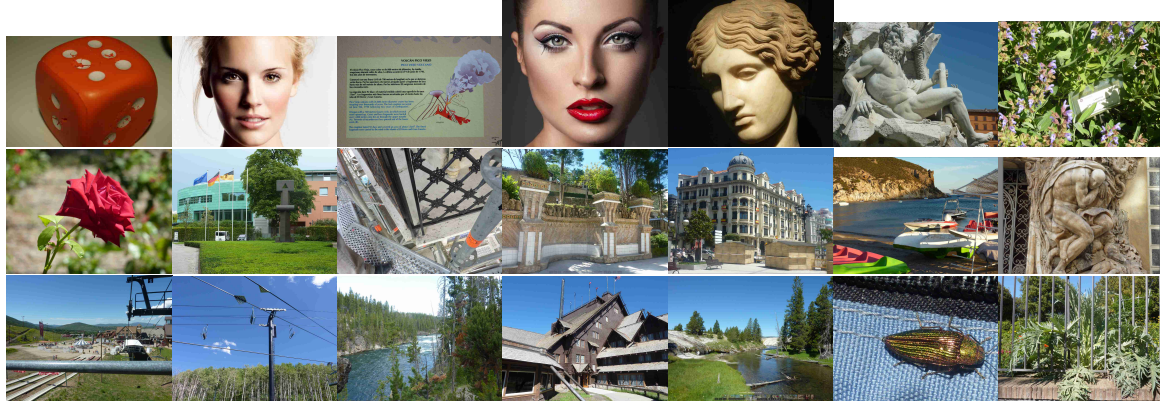


Figure 6. Training image set used to find the best parameters of each multiscale algorithm. The size of each image is about 1.5 megapixels.

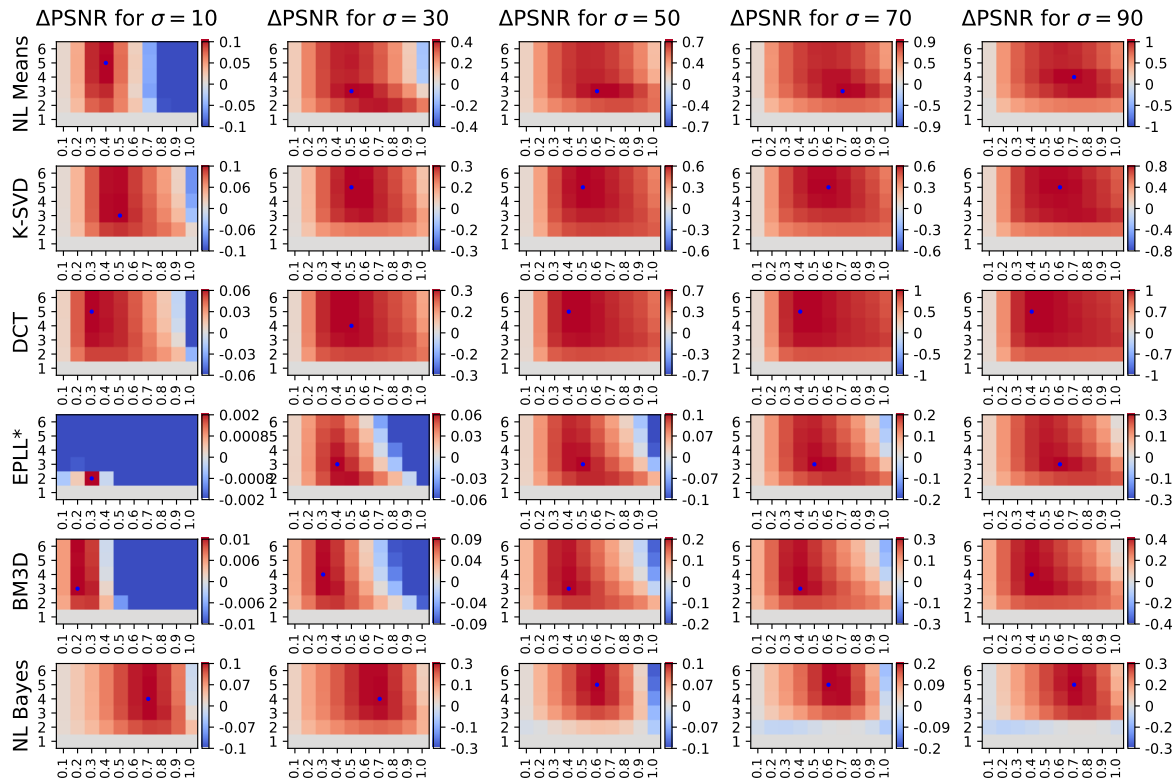


Figure 7. Average PSNR changes (in dB) obtained when varying the parameters of the DCT multiscale framework applied to several denoising algorithms with all the usual noise levels. The integers on the left of each figure (1, 2, ..., 6) represent the number of scales n_{scales} used in Algorithm 1. The bottom row of each graphic corresponds to the single-scale algorithm, for which therefore $\Delta \text{PSRN} = 0$. The value at the bottom is the fraction f_{rec} of low frequencies being used at each scale for the recomposition. Note that EPILL* was trained on grayscale images, so the actual noise standard deviations are about 0.67 times those shown in the graph.

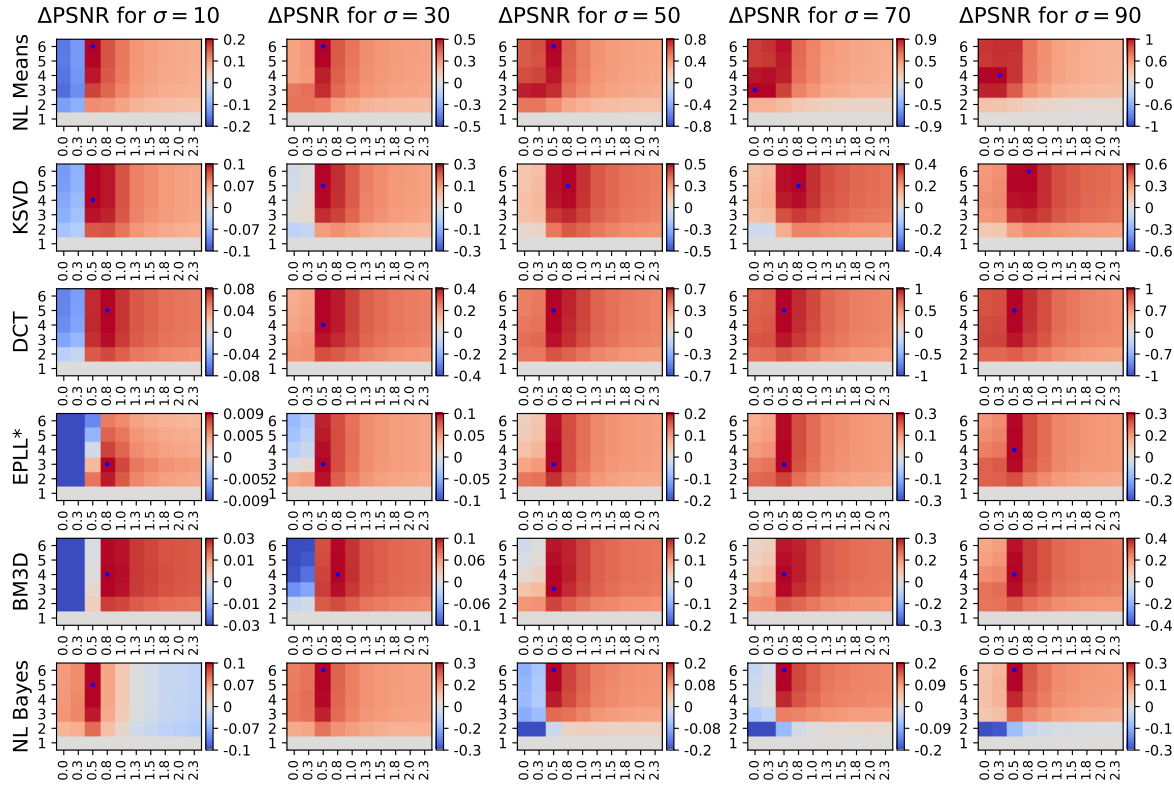


Figure 8. Average PSNR changes (in dB) obtained when varying the parameters of the Laplacian multiscale framework applied to several denoising algorithms with a sample of the usual noise levels. The integers on the left of each figure (1, 2, ..., 6) represent the number of scales n_{scales} used in Algorithm 1. The bottom row of each graphic corresponds to the single-scale algorithm for which, therefore, $\Delta \text{PSRN} = 0$. The value at the bottom is the standard deviation γ of the low-pass filtering Gaussian used in the conservative recomposition. Note that EPLL* is trained on grayscale images, so the actual noise standard deviations are about 0.67 times those shown in the graph.

followed by an aggregation of the resulting patches. The implementation used for the experiments uses smaller 8×8 patches instead of the suggested 16×16 size for the single-scale algorithm. Notice that the best results are obtained with a large number of scales. Indeed, using small patches allows the algorithm to “see” only the high frequency noise. As we shall find in the experimental evaluation, DCT denoising is spectacularly up-graded by the multiscale framework, and becomes a valid solution for low complexity requirements.

EPLL*. The conference paper [35] contains an external denoising algorithm based on a Gaussian mixture model learned from a very large set of patches sampled from noiseless images. This GMM models the patch prior. The denoising method then maximizes the Expected Patch Log Likelihood (EPLL) while being close to the corrupted image. Since the available implementation of EPLL only handles grayscale images, the noisy images are converted into grayscale before denoising. This conversion effectively reduces the noise standard deviation by a factor of 0.67, which is the geometric mean of



Figure 9. Testing image set used for the evaluation of the denoising algorithms and their multiscale versions. The size of each image is about 1.5 megapixels.

the RGB-to-luminance coefficients.

BM3D. The paper [4] is based on the fact that an image has a locally sparse representation in a transform domain. This sparsity is enhanced by grouping similar 2-D image patches into three-dimensional (3-D) groups that are jointly denoised. It is considered a reference for the performance of denoising algorithms. Even though it can provide results that contain artifacts, especially with high levels of noise, it provides high PSNR values and overall a good image quality. For low noise ($\sigma = 10$) the multiscale improvement is limited. This may be due to the fact that BM3D is highly optimized, especially for low levels of noise, and because the multiscale framework is only marginally useful with those levels of noise, since the low-resolution layers are almost noise-free.

Nonlocal Bayes. The paper [14] contains another state-of-the-art algorithm based on patch group denoising. It is fast and provides good results, both visually and in terms of PSNR. Figure 8 shows how the parameter landscape evolves with the noise level (notably starting at $\sigma = 50$). This is again due to the different parametrization of the algorithm depending on the noise levels.

Figures 7 and 8 indicate that for all methods, disabling the conservative recombination by setting $f_{rec} = 1$ (or $g_\gamma = 0$) is never optimal and always leads to suboptimal (and sometimes worse) results. Overall, the quality loss can reach -0.3 dB, which is not seen in the figure because of the restricted color code. With the optimal parameters (which are different from method to method) the PSNR (as well as SSIM) never decrease.

We observe that the optimal parameters are quite stable for different levels of noise. In general, for noise levels above $\sigma = 30$, using four scales and setting $f_{rec} \simeq 0.5$ for the DCT pyramid, and four scales and setting $g_\gamma \simeq 0.5$ for the Laplacian pyramid, seems to be a good compromise for all the considered denoising algorithms. The experiments of the next section will confirm these observations.

4. Experimental evaluation. In section 3, we identified for each considered denoising algorithm the optimal parameters that gave the best results on the training set of images shown in Figure 6. To validate the performance gain of our multiscale framework, we used a different set of images, shown in Figure 9.

The results for the DCT pyramid multiscale are shown in Table 1. For the Laplacian

Table 1

Average PSNR (expressed in decibels, dB) on the test image database (shown in Figure 9) obtained using the best trained DCT pyramid multiscale parameters for every algorithm. The standard deviations for the PSNR range from 0.1 dB for low noise values to 0.5 dB for the high ones. Note that the EPLL* algorithm is trained on grayscale images, so the actual noise standard deviation is about 0.67σ of those shown in the table.

Noise σ	NL-Means			K-SVD			DCT		
	single	multi	gain	single	multi	gain	single	multi	gain
10	35.78	35.89	0.10 ± 0.11	36.95	37.05	0.10 ± 0.11	37.01	37.07	0.05 ± 0.05
30	29.82	30.40	0.58 ± 0.32	31.04	31.31	0.27 ± 0.19	31.02	31.29	0.27 ± 0.21
50	27.00	28.06	1.05 ± 0.32	28.36	28.88	0.52 ± 0.33	28.35	28.85	0.51 ± 0.35
70	25.37	26.70	1.33 ± 0.29	26.83	27.39	0.56 ± 0.27	26.59	27.36	0.77 ± 0.46
90	24.12	25.59	1.47 ± 0.30	25.62	26.34	0.72 ± 0.38	25.26	26.29	1.03 ± 0.56
Noise σ	EPLL*			BM3D			NL-Bayes		
	single	multi	gain	single	multi	gain	single	multi	gain
10	38.02	38.02	0.00 ± 0.00	37.35	37.36	0.01 ± 0.02	37.03	37.19	0.16 ± 0.06
30	32.16	32.19	0.03 ± 0.04	31.81	31.86	0.05 ± 0.06	31.36	31.66	0.29 ± 0.09
50	29.60	29.68	0.09 ± 0.07	29.26	29.37	0.11 ± 0.09	29.42	29.57	0.14 ± 0.17
70	27.99	28.15	0.16 ± 0.10	27.81	27.96	0.15 ± 0.12	27.75	27.95	0.19 ± 0.20
90	26.83	27.08	0.24 ± 0.14	26.55	26.76	0.21 ± 0.15	26.51	26.91	0.40 ± 0.35

Table 2

Average SSIM on the test image database (shown in Figure 9) obtained using the best trained DCT pyramid multiscale parameters for every algorithm. The standard deviations for the SSIM range from 0.001 for low noise values to 0.05 for the high ones. Note that the EPLL* algorithm is trained on grayscale images, so the actual noise standard deviation is about 0.67σ of those shown in the table.

Noise σ	NL-Means			K-SVD			DCT		
	single	multi	gain	single	multi	gain	single	multi	gain
10	0.985	0.988	0.003 ± 0.002	0.988	0.991	0.002 ± 0.002	0.989	0.991	0.001 ± 0.001
30	0.925	0.952	0.027 ± 0.017	0.946	0.961	0.015 ± 0.012	0.942	0.960	0.018 ± 0.013
50	0.857	0.912	0.056 ± 0.035	0.887	0.928	0.041 ± 0.032	0.880	0.925	0.045 ± 0.034
70	0.794	0.875	0.080 ± 0.047	0.850	0.896	0.046 ± 0.035	0.813	0.890	0.077 ± 0.056
90	0.741	0.842	0.101 ± 0.048	0.798	0.866	0.068 ± 0.053	0.749	0.856	0.107 ± 0.078
Noise σ	EPLL*			BM3D			NL-Bayes		
	single	multi	gain	single	multi	gain	single	multi	gain
10	0.993	0.993	0.000 ± 0.000	0.991	0.992	0.000 ± 0.000	0.990	0.992	0.002 ± 0.001
30	0.965	0.968	0.003 ± 0.002	0.963	0.965	0.002 ± 0.002	0.954	0.965	0.011 ± 0.005
50	0.928	0.938	0.009 ± 0.006	0.930	0.936	0.006 ± 0.005	0.922	0.935	0.012 ± 0.009
70	0.891	0.907	0.016 ± 0.011	0.898	0.907	0.010 ± 0.008	0.885	0.897	0.013 ± 0.009
90	0.854	0.879	0.025 ± 0.016	0.863	0.879	0.017 ± 0.013	0.850	0.876	0.025 ± 0.020

pyramid they are shown in Table 3. The SSIM index [32] (shown in Tables 2 and 4) reflects, perhaps more specifically, the human perception of the artifacts introduced by local patch based methods, as well as ringing artifacts, which often make a small contribution to a decrease in PSNR (which quantifies only elementwise differences).

Table 3

Average PSNR (expressed in decibels, dB) on the test image database (shown in Figure 9) obtained using the best trained Laplacian pyramid multiscale parameters for every algorithm. The standard deviations for the PSNR range from 0.1 dB for low noise values to 0.5 dB for the high ones. Note that the EPLL* algorithm is trained on grayscale images, so the actual noise standard deviation is about 0.67σ of those shown in the table.

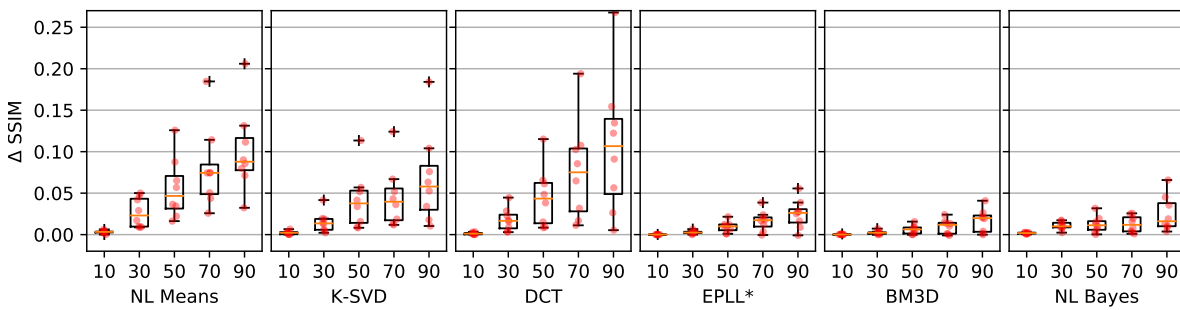
Noise σ	NL-Means			K-SVD			DCT		
	single	multi	gain	single	multi	gain	single	multi	gain
10	35.78	36.04	0.26 ± 0.12	36.96	37.07	0.11 ± 0.13	37.01	37.10	0.09 ± 0.06
30	29.82	30.54	0.72 ± 0.26	31.04	31.27	0.23 ± 0.20	31.02	31.35	0.33 ± 0.21
50	27.00	28.04	1.04 ± 0.25	28.36	28.77	0.42 ± 0.28	28.35	28.93	0.59 ± 0.32
70	25.37	26.65	1.28 ± 0.26	26.84	27.17	0.33 ± 0.25	26.59	27.45	0.86 ± 0.43
90	24.12	25.55	1.42 ± 0.26	25.62	26.11	0.48 ± 0.33	25.26	26.40	1.14 ± 0.54
Noise σ	EPLL*			BM3D			NL-Bayes		
	single	multi	gain	single	multi	gain	single	multi	gain
10	38.02	38.03	0.00 ± 0.01	37.35	37.37	0.02 ± 0.03	37.03	37.25	0.22 ± 0.04
30	32.16	32.21	0.06 ± 0.04	31.81	31.90	0.09 ± 0.06	31.36	31.72	0.35 ± 0.09
50	29.60	29.75	0.15 ± 0.08	29.26	29.41	0.15 ± 0.10	29.42	29.55	0.13 ± 0.11
70	27.99	28.22	0.23 ± 0.11	27.81	28.01	0.20 ± 0.14	27.76	27.96	0.20 ± 0.22
90	26.83	27.13	0.30 ± 0.14	26.55	26.85	0.30 ± 0.16	26.51	26.80	0.29 ± 0.28

Table 4

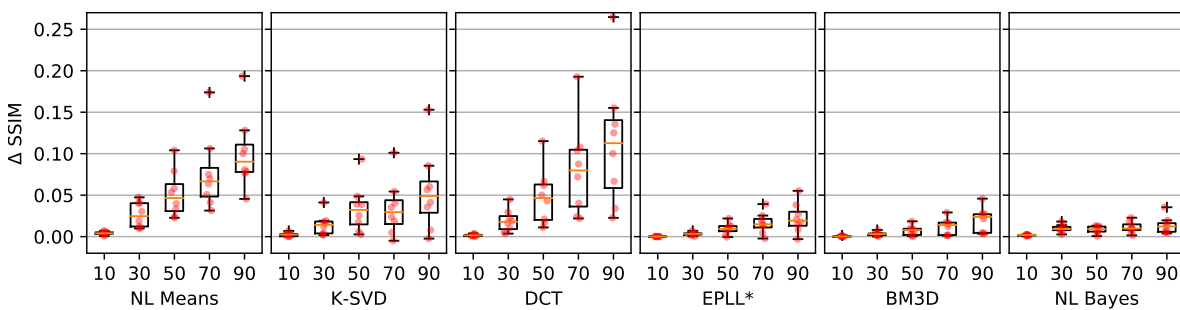
Average SSIM on the test image database (shown in Figure 9) obtained using the best trained Laplacian pyramid multiscale parameters for every algorithm. The standard deviations for the SSIM range from 0.001 for low noise values to 0.05 for the high ones. Note that the EPLL* algorithm is trained on grayscale images, so the actual noise standard deviation is about 0.67σ of those shown in the table.

Noise σ	NL-Means			K-SVD			DCT		
	single	multi	gain	single	multi	gain	single	multi	gain
10	0.985	0.989	0.004 ± 0.002	0.988	0.991	0.002 ± 0.002	0.989	0.991	0.002 ± 0.001
30	0.925	0.952	0.026 ± 0.014	0.946	0.960	0.014 ± 0.012	0.942	0.962	0.019 ± 0.013
50	0.857	0.909	0.052 ± 0.027	0.887	0.921	0.034 ± 0.027	0.880	0.928	0.048 ± 0.032
70	0.794	0.871	0.076 ± 0.043	0.850	0.885	0.034 ± 0.031	0.813	0.894	0.081 ± 0.053
90	0.742	0.843	0.101 ± 0.042	0.798	0.853	0.055 ± 0.046	0.749	0.862	0.113 ± 0.073
Noise σ	EPLL*			BM3D			NL-Bayes		
	single	multi	gain	single	multi	gain	single	multi	gain
10	0.993	0.993	0.000 ± 0.000	0.991	0.992	0.000 ± 0.000	0.990	0.992	0.002 ± 0.001
30	0.965	0.968	0.003 ± 0.002	0.963	0.966	0.003 ± 0.002	0.954	0.964	0.010 ± 0.004
50	0.929	0.938	0.010 ± 0.006	0.930	0.937	0.007 ± 0.006	0.922	0.931	0.008 ± 0.004
70	0.891	0.907	0.016 ± 0.012	0.898	0.909	0.012 ± 0.009	0.885	0.896	0.011 ± 0.006
90	0.855	0.877	0.022 ± 0.017	0.863	0.883	0.020 ± 0.014	0.850	0.864	0.014 ± 0.010

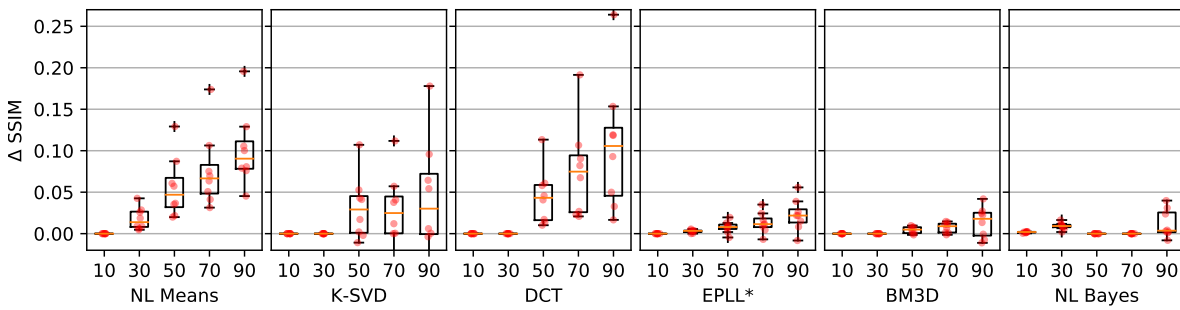
We can see from the tables that the proposed multiscale framework consistently improves the results of the single-scale version of each algorithm. This gain increases significantly with the noise level. We observe moderate gains for state-of-the-art algorithms such as BM3D and nonlocal Bayes, yielding very similar PSNR and SSIM scores after the application of the



(a) DCT pyramid with the proposed conservative recomposition.



(b) Laplacian pyramid with the proposed conservative recomposition.



(c) Laplacian pyramid as described in [2].

Figure 10. SSIM gain obtained on the test image dataset of Figure 9 applying the multiscale framework with the DCT and Laplacian pyramids with respect to the single-scale version of different denoising algorithms. Each algorithm and noise level with the corresponding optimal parameters was computed on the training images.

multiscale framework. Figures 10a and 10b illustrate the claim that the proposed multiscale framework almost never decreases the performance of the methods. The figure shows for each image the SSIM index increase resulting from applying the optimal parameters computed on the training dataset for each method.

Comparison with other multiscale algorithms. Figure 10c compares the result of our conservative recomposition strategy on a Laplacian pyramid against the meta-procedure proposed in [2], which amounts to the set $g_\gamma = 0.0$. We note that for low noise levels the optimal parameter for the procedure of [2] is to use a single scale (hence with zero gains), while

Table 5

Application of different multiscale frameworks to BM3D. We compare the Laplacian multiscale meta-procedure described in [2] with the proposed conservative recomposition applied to the DCT and the Laplacian pyramids. Note that the conservative recomposition always yields the highest PSNR gains. The results are computed using the test images shown in Figure 9.

Noise σ	BM3D single	Laplacian pyramid of [2] multi	Our Laplacian pyramid multi	Our DCT pyramid multi	gain	gain	gain
10	37.35	37.35	0.00 \pm 0.00	37.37	0.02 \pm 0.03	37.36	0.01 \pm 0.02
30	31.81	31.81	0.00 \pm 0.00	31.90	0.09 \pm 0.06	31.86	0.05 \pm 0.06
50	29.26	29.30	0.04 \pm 0.09	29.41	0.15 \pm 0.10	29.37	0.11 \pm 0.09
70	27.81	27.88	0.07 \pm 0.12	28.01	0.20 \pm 0.14	27.96	0.15 \pm 0.12
90	26.55	26.74	0.19 \pm 0.12	26.85	0.30 \pm 0.16	26.76	0.21 \pm 0.15

Table 6

Comparison with other multiscale algorithms (only grayscale results). We include the results of the DCT pyramid multiscale for the EPLL algorithm and BM3D as reference. The tests are performed on the graylevel images obtained by converting noisy color images to grayscale. This conversion reduces the noise standard deviation by a factor of 0.67. Because of that the noise levels correspond to those of the above tables times 0.67.

Noise σ	MS-KSVD [30]	MS-EPLL [21]	EPLL		BM3D (grayscale)	
			single	multi	single	multi
7	38.19	38.00	38.02	38.02	38.28	38.29
20	32.13	32.19	32.16	32.19	32.44	32.47
33	29.28	29.69	29.60	29.68	29.88	29.93
47	27.80	28.11	27.99	28.15	28.33	28.39
60	25.24	26.75	26.83	27.08	27.17	27.28

the improvement resulting from the use of the conservative recomposition is more consistent across noise levels and algorithms. In Table 5 we pick the results of BM3D with the different multiscale frameworks (similar conclusions can be drawn for all the methods) and observe that with the conservative recomposition, both DCT and Laplacian pyramids outperform the method of [2].

We also compared the proposed framework with two multiscale denoising algorithms: the multiscale KSVD algorithm of [30], and MS-EPLL, a two-scale extension of EPLL proposed in [21]. For this comparison we used grayscale versions of the test images. The results of the comparison are shown in Table 6, where we also included the results of our nonspecific multiscale DCT pyramid applied to EPLL and BM3D (as a reference). It is worth noting that for moderate noise levels our nonspecific multiscale DCT pyramid attains a performance similar to the (specific) MS-EPLL, and superior for high noise levels.

Visual quality. To judge the visual quality of the results of the proposed framework, some of the results for a noise of $\sigma = 50$ are shown in Figures 11–14. The images show results obtained using the DCT pyramid; the results of the Laplacian pyramid are very similar. It can be verified that the multiscale counterpart of each algorithm generally increases the contrast and enhances lower frequency details. This is due to the fact that within this framework those details are better denoised. The improvement for the simpler algorithms DCT denoising and NL-Means is spectacular: NL-Means gains systematically sharpness without introducing artifacts. The results of DCT denoising pass from unacceptable to competitive (particularly

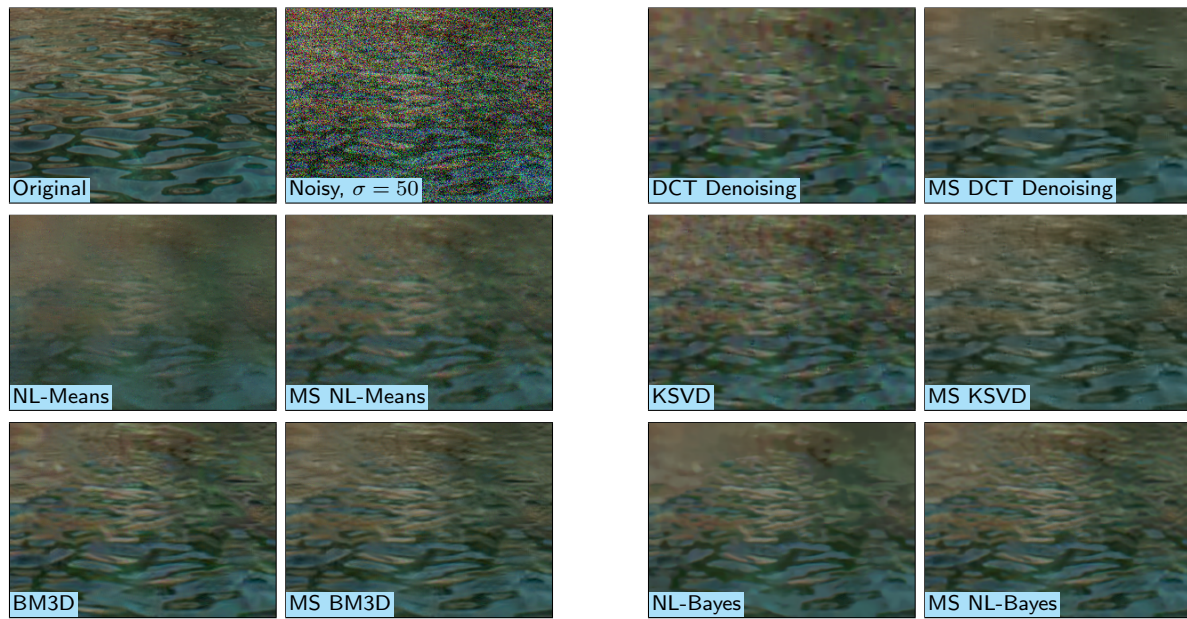


Figure 11. Results of the single-scale and multiscale (with DCT pyramid) algorithms. The details are taken from the set of test images in Figure 9. For all algorithms, one can observe a removal of spurious oscillation in smooth regions (water, glass) and a gain in detail sharpness.

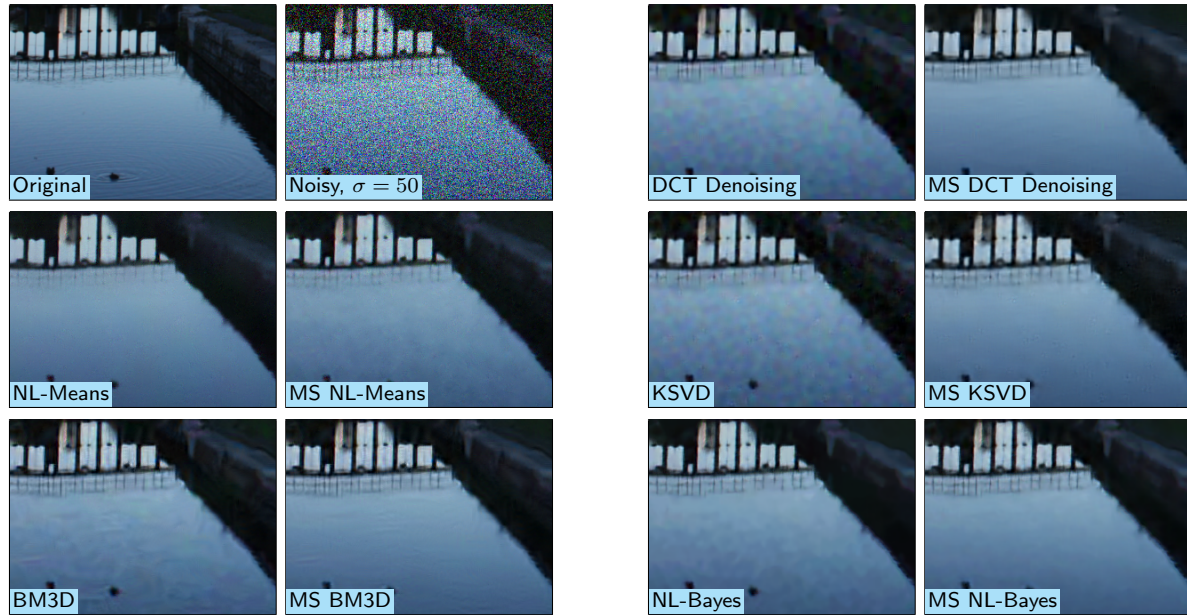


Figure 12. Results of the single-scale and multiscale (with DCT pyramid) algorithms. The details are taken from the set of test images in Figure 9. For all algorithms, one can observe a removal of spurious oscillation in smooth regions (water, glass) and a gain in detail sharpness.

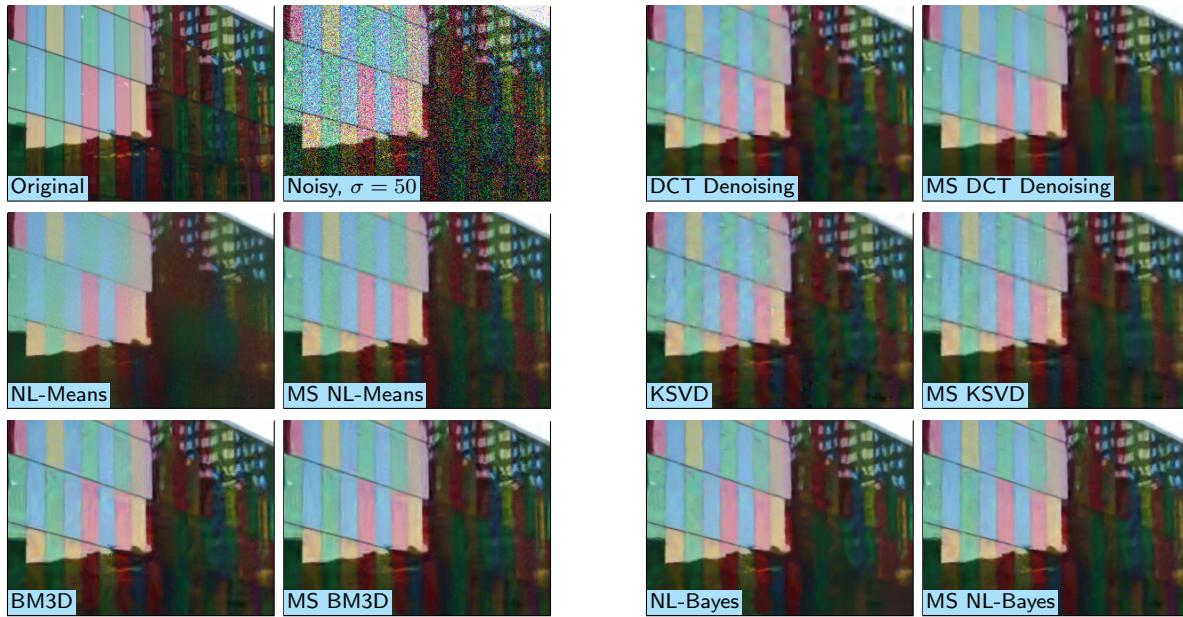


Figure 13. Results of the single-scale and multiscale (with DCT pyramid) algorithms. The details are taken from the set of test images in Figure 9. For all algorithms, one can observe a removal of spurious oscillation in smooth regions (water, glass) and a gain in detail sharpness.

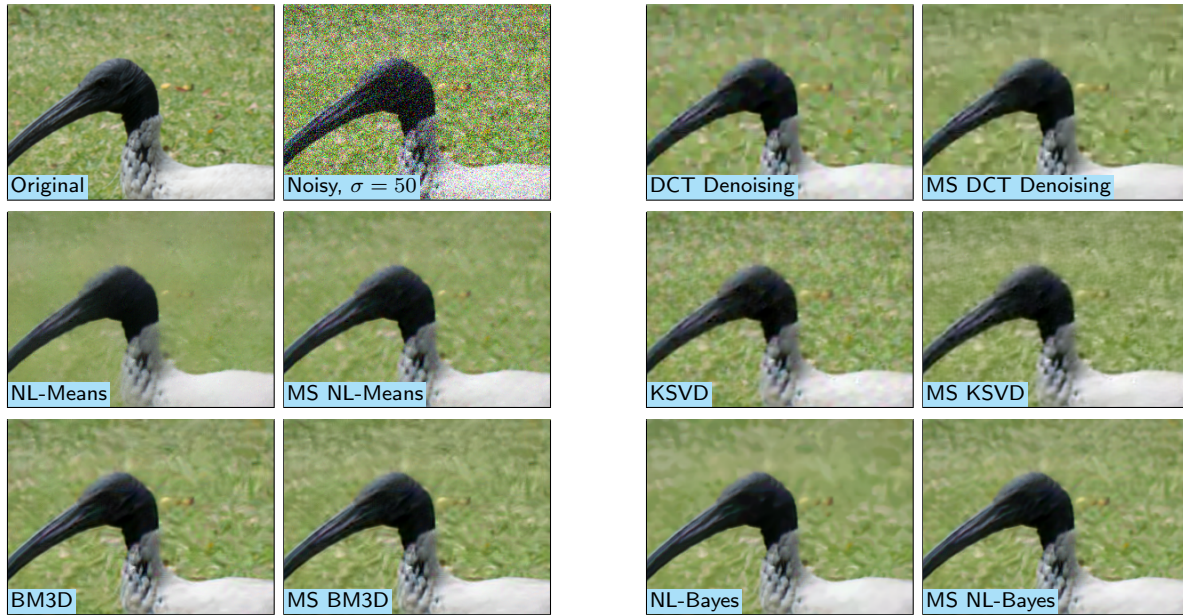


Figure 14. Results of the single-scale and multiscale (with DCT pyramid) algorithms. The details are taken from the set of test images in Figure 9. For all algorithms, one can observe a removal of spurious oscillation in smooth regions (water, glass) and a gain in detail sharpness.

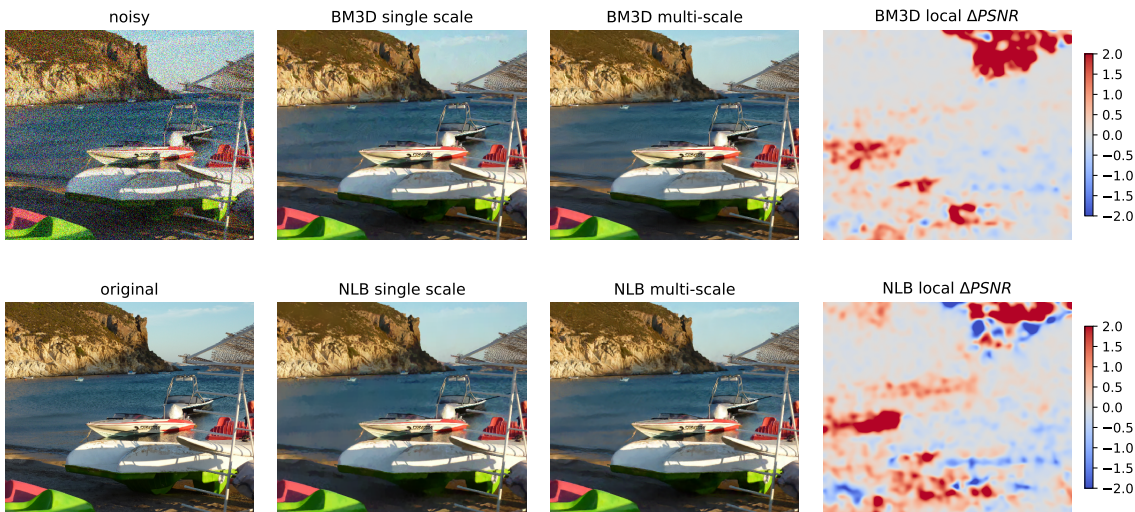


Figure 15. Local PSNR change resulting from the application of the DCT pyramid to an image with noise $\sigma = 50$. The local PSNR is computed using a Gaussian window with standard deviation of 11 pixels. The image is about 1.5 megapixels.

if we take into account the low complexity of this algorithm).

For the more complex algorithms, such as K-SVD, BM3D, and NL-Bayes, the multiscale version does indeed remove the low frequency noise. This is particularly evident in smooth areas (Figures 11 and 12), but it is also visible within geometric patterns (Figure 13). Also, for geometric structures, the multiscale framework better recovers the edges.

A special mention should be made of Figure 13. The multiscale version of the algorithm recovers some lines inside the windows of the building. At a first glance, this may look like the presence of ringing artifacts. In reality, looking at the original image, one can see that those structures are present in the original image too. No single-scale algorithm was able to retrieve them.

Analysis of the local PSNR variation with the multiscale procedure. Figure 15 shows the local PSNR change resulting from the application of the DCT pyramid to an image with noise $\sigma = 50$. The results for two algorithms are shown, but different algorithms have very different behaviors. For the algorithms shown in the figure one observes that flat and textured regions are improved by the multiscale procedure. Small PSNR regressions are observed near some contrasted edges in the NL-Bayes result, which are due to residual oscillation in the multiscale result. These oscillations are barely visible, as confirmed by the local SSIM measure (not shown). The resolution of this issue, which is still perceptually relevant, will be the subject of future exploration.

5. Conclusion. Our multiscale framework is easily applicable to all denoising algorithms. Nevertheless, no gain is to be expected by applying the framework on intrinsically multiscale algorithms, like those estimating scale mixtures of Gaussians in the wavelet domain [25, 10]. Indeed, their recomposition-denoising method is causal from coarse to fine. Thus

the result of our recombination would remain identical. This is also true for other multiscale causal algorithms based on patches, like the noise clinic proposed in [16].

We tested successfully the multiscale framework on six classic denoising algorithms, starting with the elementary DCT denoising, on which the gain is considerable. The method was also demonstrated on a dictionary learning algorithm (KSVD). On a pure patch based algorithm like NL-Means the gain is notable. Our approach, being totally general, also improves external denoising methods such as the GMM-based EPLL algorithm. In the same way, we also improved significantly BM3D and NL-Bayes.

A list of three “generic tools” was proposed for the “denoising cuisine” in [15], where it was claimed that they boosted indifferently all denoising algorithms. These tools were as follows: (a) apply a color transform, (b) aggregate estimates (by making the algorithm translation invariant), and (c) iterate using the first iteration’s result as oracle. Here we added the multiscale operation as a fourth generic tool. Our framework’s parameters are simple and general. We found that for all the considered denoising algorithms and for noise with standard deviation $\sigma = 30$ and above, using four scales and $f_{rec} \simeq 0.5$ for the DCT pyramid and $g_\gamma \simeq 0.5$ for the Laplacian pyramid always yielded an image improvement.

Acknowledgment. The authors would like to thank the anonymous reviewers for their helpful and constructive comments that greatly contributed to improving the final version of this paper.

REFERENCES

- [1] A. BUADES, B. COLL, AND J.-M. MOREL, *A review of image denoising algorithms, with a new one*, Multiscale Model. Simul., 4 (2005), pp. 490–530, <https://doi.org/10.1137/040616024>.
- [2] H. C. BURGER AND S. HARMELING, *Improving denoising algorithms via a multi-scale meta-procedure*, in Pattern Recognition, DAGM 2011, Lecture Notes in Comput. Sci. 6835, Springer, Berlin, Heidelberg, 2011, pp. 206–215, https://doi.org/10.1007/978-3-642-23123-0_21.
- [3] P. J. BURT AND E. H. ADELSON, *The Laplacian Pyramid as a Compact Image Code*, IEEE Trans. Commun., 31 (1983), pp. 532–540, <https://doi.org/10.1109/TCOM.1983.1095851>.
- [4] K. DABOV, A. FOI, V. KATKOVNIK, AND K. EGIAZARIAN, *Image Denoising by Sparse 3-D Transform-Domain Collaborative Filtering*, IEEE Trans. Image Process., 16 (2007), pp. 2080–2095, <https://doi.org/10.1109/TIP.2007.901238>.
- [5] D. L. DONOHO AND J. M. JOHNSTONE, *Ideal spatial adaptation by wavelet shrinkage*, Biometrika, 81 (1994), pp. 425–455, <https://doi.org/10.1093/biomet/81.3.425>.
- [6] S. DURAND AND J. FROMENT, *Artifact free signal denoising with wavelets*, in Proceedings of 2001 IEEE International Conference on Acoustics, Speech, and Signal Processing, 2001, Vol. 6, IEEE, 2001, pp. 3685–3688.
- [7] M. ELAD AND M. AHARON, *Image denoising via sparse and redundant representation over learned dictionaries*, IEEE Trans. Image Process., 15 (2006), pp. 3736–3745, <https://doi.org/10.1109/TIP.2006.881969>.
- [8] F. ESTRADA, D. FLEET, AND A. JEPSON, *Stochastic image denoising*, in Proceedings of the British Machine Vision Conference, BMVA Press, Durham, UK, 2009, pp. 117.1–117.11, <https://doi.org/10.5244/C.23.117>.
- [9] D. GNANADURAI AND V. SADASIVAM, *Image de-noising using double density wavelet transform based adaptive thresholding technique*, Int. J. Wavelets Multiresolut. Inf. Process., 03 (2005), pp. 141–152, <https://doi.org/10.1142/S0219691305000701>.

- [10] J. A. GUERRERO-COLÓN, L. MANCERA, AND J. PORTILLA, *Image restoration using space-variant gaussian scale mixtures in overcomplete pyramids*, IEEE Trans. Image Process., 17 (2008), pp. 27–41.
- [11] J. A. GUERRERO-COLÓN, E. P. SIMONCELLI, AND J. PORTILLA, *Image denoising using mixtures of gaussian scale mixtures*, in 15th IEEE International Conference on Image Processing (ICIP), IEEE, 2008, pp. 565–568.
- [12] D. K. HAMMOND AND E. P. SIMONCELLI, *Image denoising with an orientation-adaptive gaussian scale mixture model*, in 2006 IEEE International Conference on Image Processing, IEEE, 2006, pp. 1433–1436.
- [13] J. HUANG AND D. MUMFORD, *Statistics of natural images and models*, in IEEE Conference on Proceedings on Computer Vision and Pattern Recognition (CVPR), IEEE, 1999, pp. 541–547, <https://doi.org/10.1109/CVPR.1999.786990>.
- [14] M. LEBRUN, A. BUADES, AND J.-M. MOREL, *Implementation of the non-local Bayes (NL-Bayes) image denoising algorithm*, Image Processing On Line, 3 (2013), pp. 1–42, <https://doi.org/10.5201/ipol.2013.16>.
- [15] M. LEBRUN, M. COLOM, A. BUADES, AND J.-M. MOREL, *Secrets of image denoising cuisine*, Acta Numer., 21 (2012), pp. 475–576, <https://doi.org/10.1017/S0962492912000062>.
- [16] M. LEBRUN, M. COLOM, AND J.-M. MOREL, *The noise clinic: A universal blind denoising algorithm*, in 2014 IEEE International Conference on Image Processing (ICIP), IEEE, 2014, pp. 2674–2678.
- [17] M. LEBRUN AND A. LECLAIRE, *An implementation and detailed analysis of the K-SVD image denoising algorithm*, Image Processing On Line, 2 (2012), pp. 96–133, <https://doi.org/10.5201/ipol.2012.llm-ksvd>.
- [18] A. B. LEE, D. MUMFORD, AND J. HUANG, *Occlusion models for natural images: A statistical study of a scale-invariant dead leaves model*, Int. J. Comput. Vis., 41 (2001), pp. 35–59, <https://doi.org/10.1023/A:1011109015675>.
- [19] H.-Q. LI, S.-Q. WANG, AND C.-Z. DENG, *New Image Denoising Method Based Wavelet and Curvelet Transform*, 2009 WASE International Conference on Information Engineering, IEEE, 2009, <https://doi.org/10.1109/ICIE.2009.228>.
- [20] S. LYU AND E. P. SIMONCELLI, *Statistical modeling of images with fields of gaussian scale mixtures*, Advances in Neural Information Processing Systems, 19 (2007), pp. 945–952.
- [21] V. PAPYAN AND M. ELAD, *Multi-scale patch-based image restoration*, IEEE Trans. Image Process., 25 (2016), pp. 249–261.
- [22] N. PIERAZZO, J.-M. MOREL, AND G. FACCIOLO, *Multi-Scale DCT Denoising*, IPOL Image Processing On Line, preprint.
- [23] J. PORTILLA, *Full blind denoising through noise covariance estimation using gaussian scale mixtures in the wavelet domain*, in 2004 International Conference on Image Processing, ICIP'04, Vol. 2, IEEE, 2004, pp. 1217–1220.
- [24] J. PORTILLA, V. STRELA, M. J. WAINWRIGHT, AND E. P. SIMONCELLI, *Adaptive wiener denoising using a gaussian scale mixture model in the wavelet domain*, in 2001 International Conference on Image Processing, Vol. 2, IEEE, 2001, pp. 37–40.
- [25] J. PORTILLA, V. STRELA, M. J. WAINWRIGHT, AND E. P. SIMONCELLI, *Image denoising using scale mixtures of Gaussians in the wavelet domain*, IEEE Trans. Image Process., 12 (2003), pp. 1338–1351, <https://doi.org/10.1109/TIP.2003.818640>.
- [26] J. PORTILLA, V. STRELA, M. J. WAINWRIGHT, AND E. P. SIMONCELLI, *Image denoising using scale mixtures of gaussians in the wavelet domain*, IEEE Trans. Image Process., 12 (2003), pp. 1338–1351.
- [27] U. RAJASHEKAR AND E. P. SIMONCELLI, *Chapter 11 – Multiscale denoising of photographic images*, in The Essential Guide to Image Processing, Academic Press, New York, 2009, pp. 241–261, <https://doi.org/10.1016/B978-0-12-374457-9.00011-1>.
- [28] E. P. SIMONCELLI, *Bayesian denoising of visual images in the wavelet domain*, in Bayesian Inference in Wavelet-Based Models, Lecture Notes in Statist. 141, Springer, New York, 1999, pp. 291–308.
- [29] V. STRELA, J. PORTILLA, AND E. P. SIMONCELLI, *Image denoising using a local gaussian scale mixture model in the wavelet domain*, in International Symposium on Optical Science and Technology, International Society for Optics and Photonics, SPIE, Bellingham, WA, 2000, pp. 363–371.
- [30] J. SULAM, B. OPHIR, AND M. ELAD, *Image denoising through multi-scale learnt dictionaries*, in 2014 IEEE International Conference on Image Processing (ICIP), 2014, pp. 808–812, <https://doi.org/10.1109/ICIP.2014.7025162>.

- [31] M. J. WAINWRIGHT AND E. P. SIMONCELLI, *Scale mixtures of gaussians and the statistics of natural images*, in Proceedings of the 12th International Conference on Neural Information Processing Systems, MIT Press, Cambridge, MA, 1999, pp. 855–861.
- [32] Z. WANG, A. BOVIK, H. SHEIKH, AND E. P. SIMONCELLI, *Image quality assessment: From error visibility to structural similarity*, IEEE Trans. Image Process., 13 (2004), pp. 600–612.
- [33] C. WEN-HSIUNG, C. SMITH, AND S. FRALICK, *A fast computational algorithm for the discrete cosine transform*, IEEE Trans. Commun., 25 (1977), pp. 1004–1009, <https://doi.org/10.1109/TCOM.1977.1093941>.
- [34] G. YU AND G. SAPIRO, *DCT image denoising: A simple and effective image denoising algorithm*, Image Processing On Line, 1 (2011), pp. 292–296, <https://doi.org/10.5201/ipol.2011.ys-dct>.
- [35] D. ZORAN AND Y. WEISS, *From learning models of natural image patches to whole image restoration*, in 2011 IEEE International Conference on Computer Vision, IEEE, 2011, pp. 479–486.
- [36] D. ZORAN AND Y. WEISS, *Natural images, gaussian mixtures and dead leaves*, in Proceedings of the 25th International Conference on Neural Information Processing Systems, 2012, pp. 1736–1744.